

Intermittent contact resonance atomic force microscopy

This content has been downloaded from IOPscience. Please scroll down to see the full text.

2014 Nanotechnology 25 245702

(<http://iopscience.iop.org/0957-4484/25/24/245702>)

View [the table of contents for this issue](#), or go to the [journal homepage](#) for more

Download details:

IP Address: 129.6.130.14

This content was downloaded on 27/05/2014 at 13:18

Please note that [terms and conditions apply](#).

Intermittent contact resonance atomic force microscopy

Gheorghe Stan and Richard S Gates

Material Measurement Laboratory, National Institute of Standards and Technology, Gaithersburg, Maryland 20899, USA

E-mail: gheorghe.stan@nist.gov

Received 23 December 2013, revised 10 April 2014

Accepted for publication 24 April 2014

Published 23 May 2014

Abstract

The intermittent contact resonance atomic force microscopy (ICR-AFM) mode proposed here is a new frequency modulation technique performed in scanning force controlled AFM modes like force volume or peak force tapping. It consists of tracking the change in the resonance frequency of an eigenmode of a driven AFM cantilever during scanning as the AFM probe intermittently contacts a surface at a controlled applied maximum force (setpoint). A high speed data capture was used during individual oscillations to obtain detailed contact stiffness–force curve measurements on a two-phase polystyrene/poly(methyl methacrylate) film with sub-micrometer size domains. Through a suitable normalization, the measurements were analyzed by linear fits to provide an improved quantitative characterization of these materials in terms of their elastic moduli and adhesive properties.

Keywords: intermittent contact resonance, atomic force microscopy, nanoscale contact mechanics

(Some figures may appear in colour only in the online journal)

1. Introduction

Atomic force microscopy (AFM)-based techniques developed for measurement of elastic moduli of materials at the nanoscale aim to quantitatively interpret how the tip–sample contact-coupling quasi-statically or dynamically modifies the mechanical behavior of an AFM cantilever. The most common quantity sought in such measurements is the so-called contact stiffness, which models the spring-coupling between an AFM tip and the sample probed. The contact stiffness can be retrieved either from the slope of force–displacement curves made either at slow rate (force volume AFM [1]) or high rate (Harmonix [2], pulsed-force mode [3], peak force tapping (PFT) [4]) or from the change in the resonance frequency of the cantilever (contact-resonance AFM [5, 6] and amplitude-modulation frequency-modulation AFM [7]). Conceivably, other quantities could be used to observe how the cantilever mechanics is perturbed by the tip–sample contact-coupling. These include amplitude (e.g. ultrasonic force microscopy [8]) and phase (e.g. resonant difference-frequency atomic force ultrasonic microscopy [9]) imaging using a mechanically vibrated AFM probe brought in contact

with a material. However, various contributions from the tip–sample interaction (elastic, viscoelastic, adhesive) are convoluted into amplitude and phase information so it is more difficult to separate these contributions and determine them from single imaging scans.

With elastic moduli measurements ranging from few GPa to hundreds of GPa, contact resonance AFM (CR-AFM) classifies as one of the most versatile AFM-base technique for nanoscale elastic modulus measurements. It has proven to be a robust technique for nanoscale elastic modulus measurements, with applications on various composites [10, 11], thin films [12], and nanostructures [13, 14]. Nominally, CR-AFM is a contact AFM mode and it is used mostly in the relative mode, with measurements made successively on the test material and a reference material (with known elastic modulus) at a predefined applied force. An improvement in CR-AFM accuracy has been demonstrated by performing measurements not only at a given applied force but over the entire contact range as the AFM probe is brought in and out of contact with a material [15, 16]. An immediate extension of this type of point-measurements is to accommodate depth-dependent CR-AFM measurements during force-volume

AFM scans to obtain three-dimensional (3D) mechanical property characterizations [17] with the drawback of a slow rate. Therefore, tracking the contact resonance frequency during fast scanning modes like intermittent-contact AFM modes has been a quest during the last few years.

One approach would be to develop a fast resonance frequency tracking on the basis of various frequency and amplitude-modulation AFM techniques. Besides fast topographical scans, these intermittent-contact AFM modes were sought also to provide mechanical property characterization in terms of conservative and dissipative tip-sample interactions. Thus, in the amplitude-modulation AFM (AM-AFM also known as tapping mode [18, 19]), the phase was considered [20, 21] to provide qualitative contrast associated with the energy dissipation, although it is not straightforward to deconvolute its various topographic, adhesive, elastic, and viscoelastic contributions. In the last ten years a better separation between conservative and dissipative contributions was thought to be possible in the new developed multi-frequency-modulation AFM modes [22–27]. The idea of multifrequency-modulation AFM modes is to use one eigenmode (usually the first eigenmode) as a carrier mode to track the topography like in AM-FM and simultaneously excite one or more higher eigenmodes to observe the elastic and viscoelastic responses of the sample probed. While these methods introduced interesting avenues of imaging various materials, several issues are still to be solved for proper quantitative mechanical property measurements: force control during intermittent contact, adhesive force measurement, and force-resonance frequency correlation during contacts (due to the fast dynamics, the frequency shifts are measured over many oscillations and don't reflect the momentarily variation in the tip-sample interaction during individual oscillations).

In this work, we propose an intermittent contact resonance (ICR) AFM method to retrieve force-frequency measurements during individual oscillations of an intermittent-contact AFM mode, namely PFT. In this new method the induced change in the resonance frequency of a cantilever eigenmode due to the change in the tip-sample interaction is measured progressively as the tip is brought in and out of contact with the sample. Because PFT is a force controlled AFM mode, the frequency measurements can be synchronized with the applied force during tip-sample interaction, so a more robust confirmation of the contact mechanics can be extracted from the measured force dependence of the contact stiffness. The dynamics of ICR-AFM has the potential to add new features to the mechanical characterization provided by the quasi-static PFT force-distance curve measurements: (1) contact stiffness measurements at each indentation depth, which gives a detailed 3D elastic response of the material; (2) detailed observation of the tip-sample interaction around contact formation and contact breaking, which can be used for adhesive property characterization; (3) dynamic characterization of the dissipated energy during tip-sample interaction, both in and out of contact.

Through the use of the dynamics of one of its eigenmodes, ICR-AFM complements other existing intermittent and non-contact AFM techniques, like amplitude modulation

AFM (AM-AFM) [18, 19] and frequency modulation AFM (FM-AFM) [28, 29]. In AM-AFM, the modulation is made at a fixed frequency (e.g. at or near to the first free-resonance frequency of the cantilever in tapping mode) and the tapping amplitude is maintained at a constant level through a feedback loop by adjusting the relative tip-sample distance; the amplitude loop provides the z-topographical profile of the scanned area. In non-contact FM-AFM, in addition to the amplitude feedback (also used to observe non-conservative forces) the modulation frequency is maintained at resonance through a separate loop that provides measurement of the conservative tip-sample interactions. Lately, FM-AFM was extended to provide 3D high-resolution imaging of the force field above the sample surface [30, 31]. Like FM-AFM, the frequency modulation loop in ICR-AFM is used to retrieve the tip-sample interactions but mainly in contact. Unlike FM-AFM where small frequency shifts (order of Hz) detail the non-contact interactions, large frequency shifts in ICR-AFM (order of kHz) are induced and indicative of the tip-sample contact deformation. Ultimately, ICR-AFM can be used for 3D mapping of the nearby subsurface elastic field in a similar way as force volume contact resonance [17]. In this work, the scope is limited to demonstrating the applicability of ICR-AFM for quantitative nanoscale mechanical property characterization of a two-phase polystyrene/poly(methyl methacrylate) (PS/PMMA) film with emphasize on measuring the elastic and adhesive responses of the two materials.

2. Experimental methods

Here, we demonstrate a new high-speed ICR-AFM mode capable of tracking the change in the resonance frequency of an eigenmode of a vibrating AFM cantilever during individual oscillations (taps) as the AFM probe intermittently contacts a surface during a fast scanning (imaging) mode. The scanning mode used was PFT, which provides an intermittent contact mode at frequencies on the order of a few kHz and feedback control for the maximum applied force (peak force). Unlike PFT, the common tapping mode (AM-AFM) [18, 19] operates at the first eigenmode frequency of the cantilever, tens or hundreds of kHz, and uses feedback control on amplitude modulation (not on force). Thus, the high-speed operation and lack of force control make AM-AFM unsuitable for observing reliable tip-sample interaction during individual taps. In this work, the PFT was paired with high-speed phase-locked loop (PLL) instrumentation for independently tracking the change in the resonance frequency of the cantilever. The key point in ICR-AFM is that the force-distance curves from PFT can be precisely synchronized with the resonance frequency measurements from PLL, so a contact stiffness versus force (or distance) curve can be obtained at any point in the scan. Previous attempts [32] of tracking the contact resonance frequency during the oscillations of an intermittent scanning mode have been made in a pulsed-force mode but without rigorous force control. Moreover, with the characteristic ringdown vibrations of the pulsed-force oscillation, only a limited range of individual force-distance

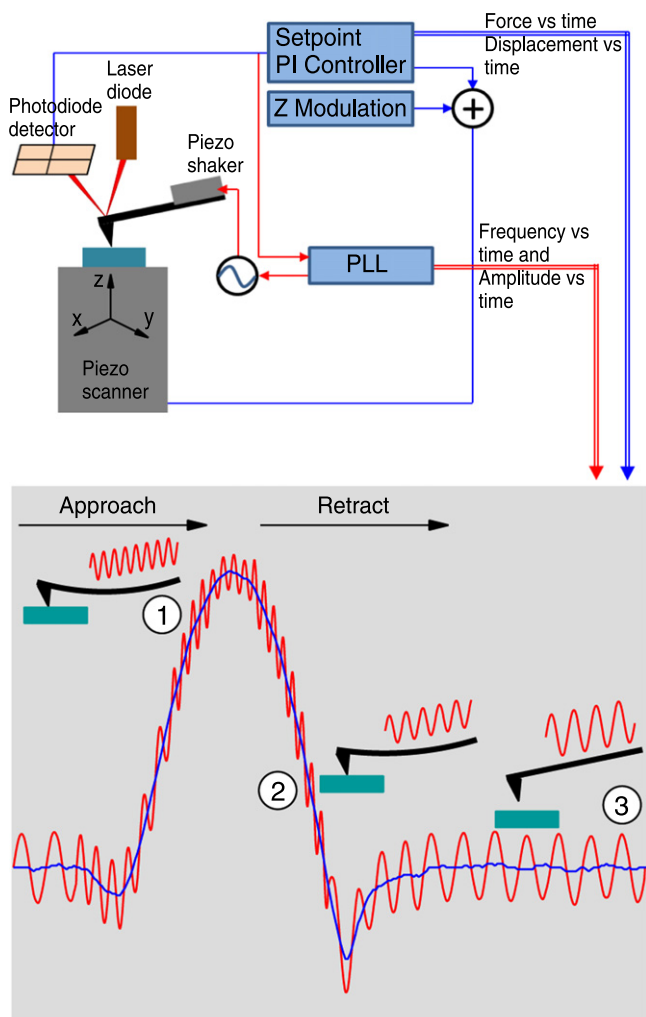


Figure 1. Schematic diagram of the new implemented ICR-AFM mode, with the amplitude modulation controlled by PFT (blue loop) and the frequency modulation controlled by PLL (red loop). The cantilever deflection during one PFT oscillation is detailed in the lower panel, as superimposed responses to the tip-sample interactions of the two excitations: slow PFT tapping oscillation (blue line) and fast PLL modulation (red line); the change in the resonance frequency of the cantilever is schematically shown at different locations along one cycle of the PFT oscillation. The acquisition of cantilever deflection and z -piezo displacement from PFT and resonance frequency and amplitude from PLL are time-correlated during each PFT oscillation.

curves was available for resonance frequency tracking and this was possible only in single-point measurements and lift-mode [32].

In the new ICR-AFM mode described in this work, the PFT amplitude modulation was operated at 2 kHz on a MultiMode V AFM (Bruker, Santa Barbara, USA)¹ with a peak force of 35 nN and modulation amplitude of 8 nm. Simultaneously, an independent frequency modulation of

¹ Certain commercial equipment, instruments, or materials are identified in this document. Such identification does not imply recommendation or endorsement by the National Institute of Standards and Technology, nor does it imply that the products identified are necessarily the best available for the purpose.

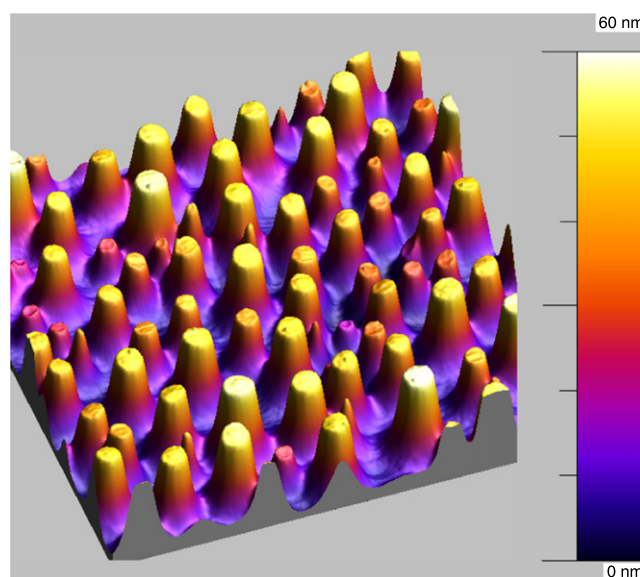


Figure 2. AFM micrograph showing the topography of a $5.0 \mu\text{m} \times 5.0 \mu\text{m}$ of the investigated PS/PMMA blend. The PMMA phase is in the form of cylindrical pillars surrounded by the PS matrix.

small amplitude was added to the cantilever and controlled by a PLL system (SPECS, Zurich, Switzerland) (see footnote 1). As shown in figure 1, the two modulations are applied to the tip-sample contact through two separated actuators and at unrelated frequencies for crosstalk reduction: the amplitude modulation is at 2 kHz (a non-eigenmode of the cantilever) and the frequency modulation is at one of the cantilever's eigenmodes (as specified below, the fast modulation was done at the third eigenmode frequency of the cantilever). The lower panel of figure 1 shows that (going from left to right) as the tip is brought in and out of contact during one PFT oscillation, the resonance frequency of the cantilever shifts from its free value to higher and higher values and goes back to its free value: at position (1), on approach, a high load imposes a high shift in the contact resonance frequency; at position (2), on retract, a lower applied load provides a lower shift in the contact resonance frequency; at position (3), the cantilever is out of contact and the resonance frequency returns to its free oscillation value.

The AFM probe used for ICR-AFM measurements was a PPP-SEIH integrated Si probe (NanoSensors, Neuchatel, Switzerland) (see footnote 1) with a cantilever spring constant of $9.12 \pm 0.07 \text{ N m}^{-1}$ (measured using a laser-Doppler vibrometer (Polytec, GmbH, Waldbronn, Germany) (see footnote 1) and thermal calibration methods developed at NIST) [33, 34]. This particular cantilever had its first three out-of-contact flexural resonance frequencies of 107.3 kHz, 670.5 kHz, and 1865.5 kHz, respectively. Measurements were made on a PS/PMMA film containing sub-micrometer size PMMA domains (figure 2) provided by Bruker-Nano (Santa Barbara, USA) (see footnote 1). The PS/PMMA blend was prepared from xylene solution mixed in 50–50 ratio; both PS (Ww-21 000, Wm-17 000) and PMMA (Ww-53 000, Wm-35 000) were from Polymer Source (Montreal,

Canada) (see footnote 1). The slight difference in the elastic moduli of the two materials (about 3.4 GPa for PS and about 3.0 GPa for PMMA) [35] is expected to provide a contrast in the resonance contact frequency response when areas encompassing both PS and PMMA regions are mapped. The uncertainties introduced by PLL in measuring the resonance frequency at the locked phase of the free resonance were calculated for a model clamped-coupled cantilever configuration that reproduced our experimental setup. For the maximum resonance frequency shifts (about 15 kHz) and amplitude damping (about 80 % from out of contact to contact) observed during measurements, the PLL uncertainties were on the order of a few tens of Hz, which is insignificant for CR-AFM conversion of kHz frequency shifts into GPa elastic moduli.

For meaningful ICR-AFM measurements, the measurement frequency (controlled here by the PLL time constant) has to be significantly higher than the tapping frequency (2 kHz) to be able to acquire enough measurement points during each oscillation (tap) but, at the same time, has to be less than the frequency of the eigenmode used to assure a good detection. To satisfy these criteria, we chose to excite the third eigenmode of the cantilever and adjusted the PLL time constant between the frequency constraints. A first example of PLL time constant adjustment is shown in figure 3 with various maps acquired either directly by PFT (topography, adhesion, dissipation, and Derjaguin, Muller, and Toporov (DMT) modulus) and feedback from PLL signals: resonance frequency tracked with a slow PLL in figure 3(e) (100 μ s time constant) and with a fast PLL in figure 3(f) (1 μ s time constant). As can be seen from the PFT maps, the PMMA appears to be less adhesive and less dissipative than PS but with no significant difference between their DMT elastic moduli. Regarding the resonance frequency maps, in figure 3(e) there is a contrast suggesting PS is stiffer than PMMA whereas in figure 3(f) the contrast between PS and PMMA is negligible. However, if we look at their frequency shift values, we can see that in the case of a faster PLL (figures 3(f) and (l)) the resonance frequency shifts are higher than those measured with a slow PLL (figures 3(e) and (k)). The explanation here is that, in both cases, the maps are showing values averaged over the time per pixel, which in the case of these scans was 1.5 ms. The signals were interrogated every 50 μ s, but only the average values over the pixel time were collected. In the case of the faster PLL detection, the average values of the resonance frequencies show the same contrast with that from the DMT modulus map, whereas in the case of a slower PLL detection, due to a larger time interval, a larger contribution comes from the contact region dominated by adhesive forces, so the contrast in the frequency map (figure 3(e) more closely resembles the adhesion map (figure 3(b)). However, the interpretation of average resonance frequency maps is qualitative at most and requires corroboration with contributing information like modulus, adhesion, and dissipation. This is similar to the case of bimodal resonance frequency mapping [7] where the amplitude modulation (tapping mode) is made at very high frequencies so the measured resonance frequency is averaged

over many oscillations, but in those cases there is no force control, and no measurement of adhesive forces. A proper interpretation of the resonance frequency response requires *both* measurements during individual oscillations and known force at each instant.

3. Results and discussion

Short scanning segments from a high speed data capture at a rate of 500 kHz over a PS region are shown in figure 4 for both slow and fast PLL detections. It can be seen that in the case of a slow PLL detection (figure 4(a)) the measured contact resonance frequency shifts are within 1 kHz from the free resonance frequency and with no significant force dependence. However, in the case of a fast PLL detection (figure 4(b)), the contact resonance frequency shows shifts as large as 15 kHz at the peak force and responds with fidelity to the force variation during each oscillation. These observations suggest the possibility of obtaining 3D characterization of the nanomechanical properties of surfaces at imaging speeds. The 3D details of the force-frequency (figure 4) or depth-frequency dependencies are not apparent in the 2D-maps shown in figures 3(e) and (f) due to the time averaging of the signals over the oscillation cycles. In the following example, we analyzed only a small data subset of measurements acquired with a fast PLL over the region marked by arrows in figure 3; the data covered 58 oscillations over PMMA and 122 oscillations over PS (on both sides of the PMMA region). The measurements are shown in figure 5(a) in the form of resonance frequency shift versus applied force. It can be seen that the resonance frequency shift provides a clear distinction between the two materials at any given force on either approach or retract portions. Since the retract portions contain additional data on the adhesion effect and detachment point, we chose those data for further modeling and analysis.

In general, the contact mechanics of adhesive contacts on perfectly elastic materials is customarily analyzed within the limits of two models that include contributions of adhesive forces: DMT model [36], which considers the contribution of long-range attractive forces outside the contact area, and Johnson, Kendall, and Roberts (JKR) model [37], which includes the contribution from attractive forces acting only inside the contact area. A more realistic interpretation relies on using a model that captures the transition regime between these two limiting cases, e.g. Maugis-Dugdale [38], Carpick-Ogletree-Salmeron [39], or Schwarz [40] models. Due to its simple analytical form and direct interpretation, we used the Schwarz model in this work to analyze the stiffness-force curves extracted from the measurements. In the Schwarz model, a transition parameter τ_1 , defined as the square root of the ratio between the work against the short-range adhesive forces and the total work of adhesion, ranges from 0 (DMT limit) to 1 (JKR limit). The force dependence of the contact

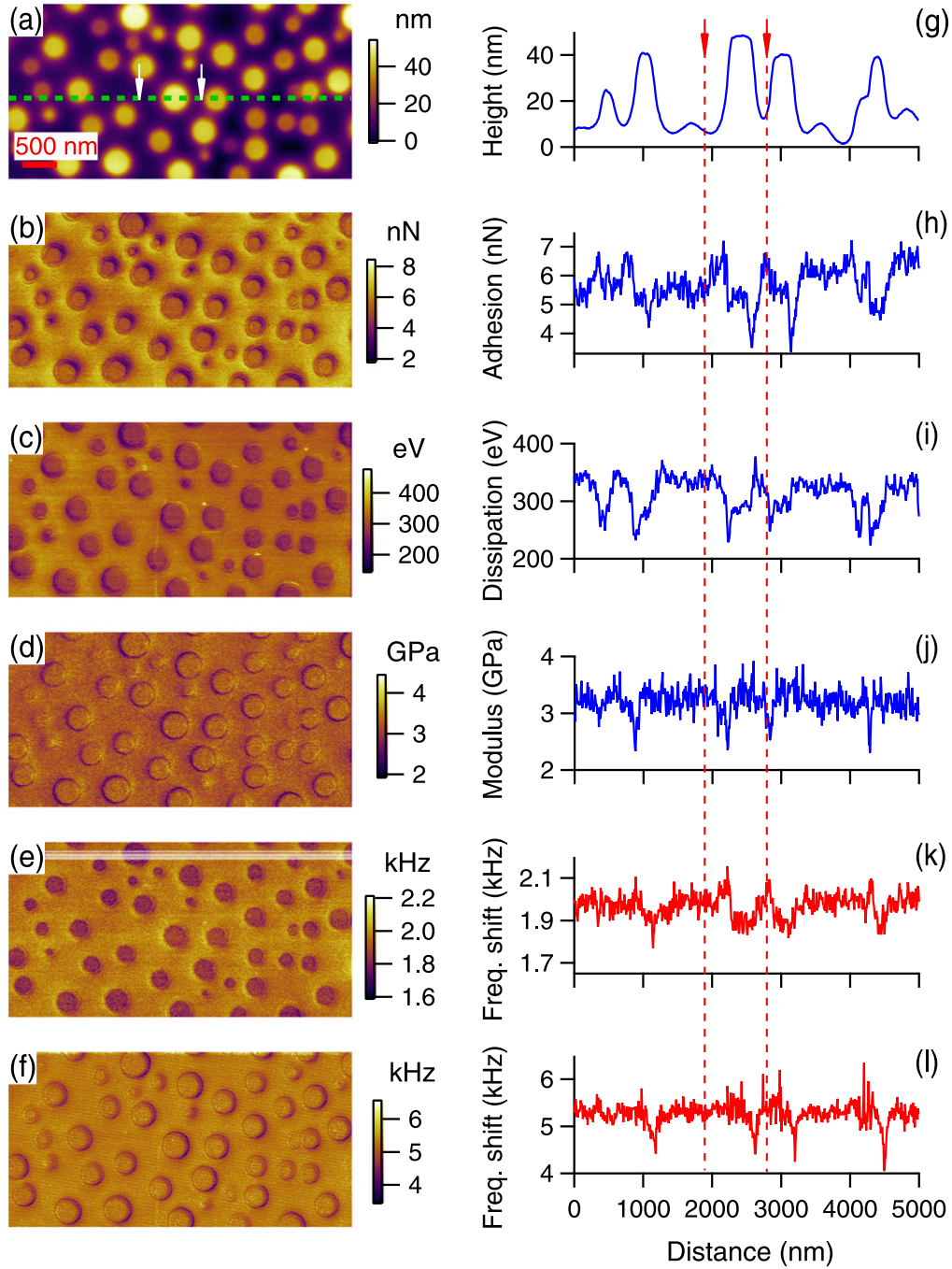


Figure 3. Maps of (a) topography, (b) adhesion, (c) dissipation, (d) DMT modulus, (e) resonance frequency shift with slow PLL, and (f) resonance frequency with fast PLL over $5 \mu\text{m} \times 2.5 \mu\text{m}$ area of the PS/PMMA sample. In these maps, the PMMA regions are visible as circles and PS as the matrix. (g)–(l) traces from each of the left maps along the dotted scan line shown in (a). DMT modulus refers here to the elastic modulus calculated by using the Derjaguin, Muller, and Toporov (DMT) model [36].

radius is given in this model by [17]

$$a = \left(\frac{3R_T}{4E^*} \right)^{1/3} \left(\frac{\tau_1}{\sqrt{4 - \tau_1^2}} \sqrt{3F_a} \pm \sqrt{F + F_a} \right)^{2/3}, \quad (1)$$

where R_T is the tip radius, F_a is the maximum adhesive force at the detachment of the tip–sample contact, and the reduced elastic modulus E^* is given in terms of the indentation

moduli of the tip and sample, $1/E^* = 1/M_T + 1/M_S$. For elastically isotropic materials the indentation modulus is simply expressed in terms of the Young's modulus E and the Poisson's ratio ν , $M = E/(1 - \nu^2)$. Since the compliances of the elastomers probed were much greater than that of Si, the deformation of the AFM tip was neglected in this study. The signs + and – indicate the stable (the tip is continuously in contact with the sample) and unstable (the

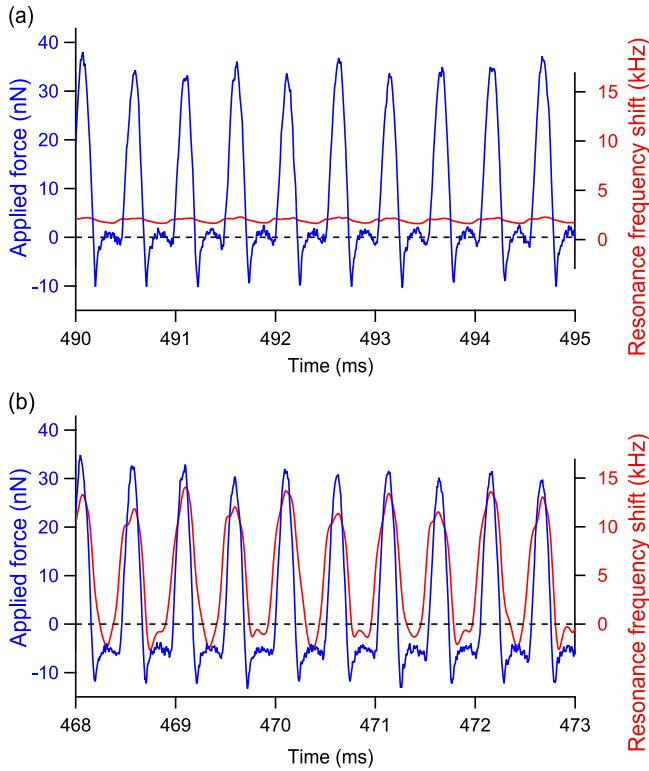


Figure 4. Force and resonance frequency shift along few successive PFT oscillations during scanning over PS. In (a) the resonance frequency shift was tracked with a slow PLL detection and in (b) a fast PLL detection was used. In each case the imaging scan speed was 1 Hz.

tip is pulling off of and away from the sample) contact regions.

A particular contact mechanics model has been proposed in the case of high speed indentation of an elastomer [41, 42]. Thus, it is expected that in the case of a fast oscillating indentation, like that imposed during ICR-AFM, viscoelastic effects will hinder the peripheral variations imposed by the oscillation onto the contact area. As a result, the contact area remains approximately constant during an oscillation and the contact geometry resembles that of a ‘flat punch’ configuration (an indenter with circular flat end). In the limit of this dynamic flat punch approximation, the expression of contact stiffness reduces to $k^* = 2aE^*$, with the contact stiffness being proportional to the contact radius a . The expression for the contact stiffness of a dynamic flat punch in the Schwarz model becomes [17]

$$k^* = (6R_1 E^{*2})^{1/3} \left(\frac{\tau_1}{\sqrt{4 - \tau_1^2}} \sqrt{3F_a} \pm \sqrt{F + F_a} \right)^{2/3}. \quad (2)$$

The equation can be rearranged to show the linear relationship between $\sqrt{F + F_a}$ and $\sqrt{k^{*3}}$:

$$\sqrt{F + F_a} = \left| \alpha \sqrt{k^{*3}} - \beta \right|, \quad (3)$$

with $\alpha = 1/\sqrt{6R_1 E^{*2}}$ and $\beta = \sqrt{3F_a} \tau_1 / \sqrt{4 - \tau_1^2}$. This linear

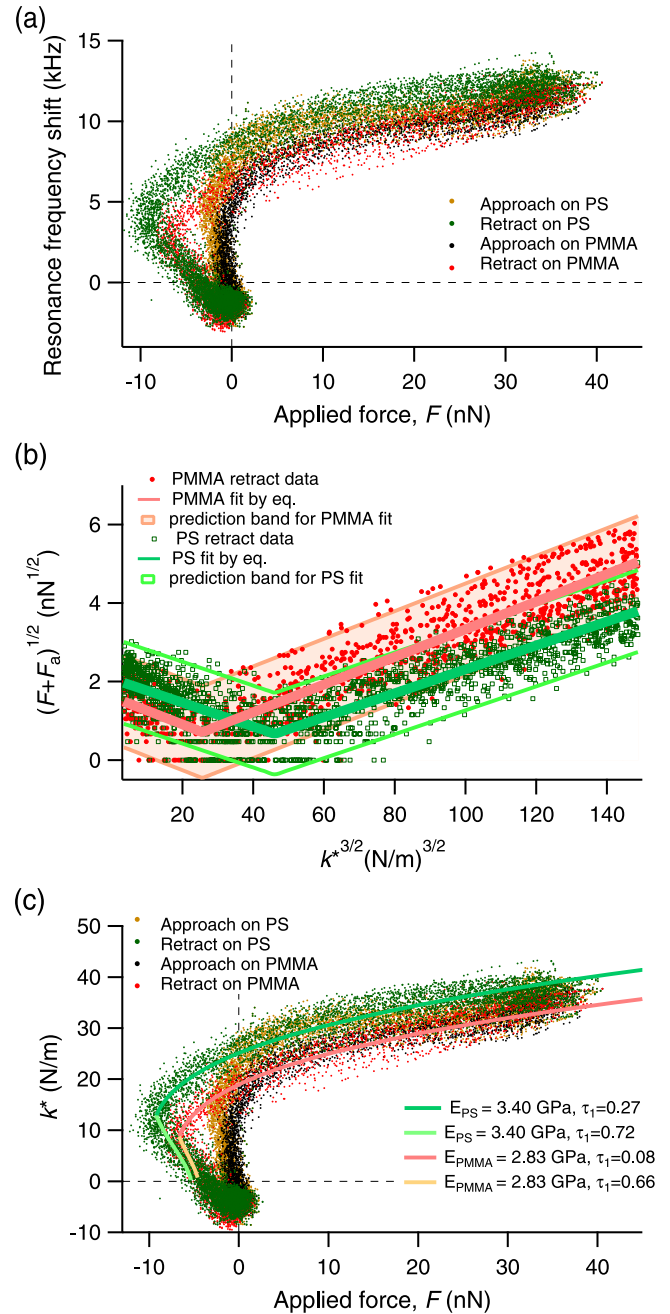


Figure 5. (a) Resonance frequency shifts versus applied force during individual oscillations of PFT along a portion of a scan line; (b) linear fits of $\sqrt{F + F_a}$ versus $\sqrt{k^{*3}}$ with 95% prediction bands; (c) measured contact stiffnesses versus applied force with the dependencies given by equation (2) for the fit parameters obtained in the linear fits shown in (b).

dependence was probed in figure 5(b) using retract data around the detachment point ($F = -F_a$) on both PS and PMMA: at the left of the detachment point the data were fit by the unstable solution and at the right of the detachment point by the stable solution. For each material, the unstable and stable regions were fitted simultaneously by considering the same value of α for both of them and a different value of β , which means a different value of τ_1 for each region. For the

fits shown in figure 5(b), the tip radius was adjusted to 12.95 nm to provide an indentation modulus of 3.73 ± 0.10 GPa for PS, which was considered as a reference material. The indentation modulus of PS was calculated by considering 3.40 GPa and 0.33 for the Young's modulus and Poisson's ratio of PS [43] respectively. With that and the measured average $F_a = 9.64$ nN, the best fit for PS data indicated a transition parameter τ_1 of 0.27 ± 0.04 for the stable branch and 0.72 ± 0.01 for the unstable branch. For PMMA, with $R_T = 12.95$ nm and $F_a = 7.17$ nN, the best fit was for an indentation modulus of 3.22 ± 0.09 GPa and a transition parameter going from 0.08 ± 0.04 for the stable branch to 0.66 ± 0.03 for the unstable branch. The determined indentation modulus of PMMA can be converted into 2.83 ± 0.08 GPa Young's modulus by considering an average Poisson's ratio of 0.35 for PMMA. All uncertainties represent one standard deviation of the calculated values. The theoretical stiffness–force curves for the found fit parameters are plotted as solid lines along with measurements in figure 5(c).

In comparison with force–distance measurements, the ICR-AFM measurements and their fits indicated an improved sensitivity in differentiating the mechanical response of the two probed elastomers. Thus, in terms of their elastic moduli, a clear difference was determined between PS (3.4 GPa) and PMMA (2.8 GPa) with ICR-AFM whereas in either individual force–distance curves (not shown here) or maps (refer to figure 3(d)) no distinct contrast between PS and PMMA was observed. The advantage of ICR-AFM over force–distance measurements is that it provides a measurement for the contact stiffness at any applied force, whereas with force–distance measurements the contact stiffness could be only calculated from the derivative of the measurements and it is not accurate around the contact point due to the reduced number of measurements. In addition, a detailed depth-dependent contact stiffness measurement provides an improved validation of the contact model used over the entire contact depth. In the present case, it was possible to differentiate the transition parameter τ_1 of the Schwarz model during contact deformation, 0.3 for PS and 0.1 for PMMA. Qualitatively, this agrees with the measurement of a smaller adhesive force on PMMA than PS. Interestingly, due to the high rate contact stiffness measurement, data were obtained in the contact detachment region, with a negative slope of stiffness versus force curve (refer to figure 5(c)). In this region, the transition parameter τ_1 has comparable values for both materials, slightly bigger on PS than PMMA, which indicates that, at least for these data sets, the response in this region is dominated by the contact geometry and less specific to material properties.

4. Conclusions

A new high-speed nanomechanical property measurement AFM technique, ICR-AFM, has been demonstrated with capabilities of interrogating surfaces during a force-controlled tapping mode. The technique utilizes fast resonance

frequency PLL tracking of a higher eigenmode of a cantilever during PFT imaging. Shifts in the resonance frequency of the third eigenmode of the cantilever were measured and correlated with the deflections of the cantilever to determine the induced changes in the tip–sample stiffness during individual PFT oscillations on a PS/PMMA blend. Besides the contact stiffness characterization, the new ICR-AFM showed very good sensitivity in resolving the adhesive response of materials, which suggests the possibility of performing a real-time characterization of the mechanics of contact formation and detachment during fast contacts on elastomers.

We have demonstrated an improved quantitative measurement of the elastic moduli of PS (3.4 GPa) and PMMA (2.8 GPa) probed in this work by collecting the depth-dependence of the contact stiffness during successive tapping oscillations while imaging. Detailed contact stiffness measurements over the entire contact depth provided robust verification of the applicability of a contact model that includes both long and short range adhesive forces. Within the proposed analysis, the mechanical differences between the two materials were demonstrated both in terms of elastic moduli and transitional parameters. Based on its quantitative mechanical property measurement capability, ICR-AFM can be used as a depth sensing technique for 3D characterization of near-surface mechanical properties of various nanocomposite materials.

Acknowledgments

The authors thank Dr Natalia Erina for sample preparation.

References

- [1] Radmacher M, Cleveland J P, Fritz M, Hansma H G and Hansma P K 1994 *Biophys. J.* **66** 4917
- [2] Sahin O, Magonov S, Su C, Quate C F and Solgaard O 2007 *Nat. Nanotechnology* **2** 507
- [3] Rosa-Zeiser A, Weilandt E, Hild S and Marti O 1997 *Meas. Sci. Technol.* **8** 1333
- [4] Pittenger B, Erina N and Su C 2010 *Bruker Appl. Note AN128* 1
- [5] Rabe U, Janser K and Arnold W 1996 *Rev. Sci. Instrum.* **67** 3281
- [6] Yamanaka K and Nakano S 1996 *Japan J. Appl. Phys.* **35** 3787
- [7] Garcia R and Proksch R 2013 *Eur. Polym. J.* **49** 1897
- [8] Yamanaka K, Ogiso H and Kolosov O 1994 *Appl. Phys. Lett.* **64** 178
- [9] Cantrell S A, Cantrell J H and Lillehei P T 2007 *J. Appl. Phys.* **101** 114324
- [10] Yamanaka K, Maruyama Y, Tsuji T and Nakamoto K 2001 *Appl. Phys. Lett.* **78** 1939
- [11] Passeri D, Bettucci A, Germano M, Rossi M, Alippi A, Sessa V, Fiori A, Tamburri E and Terranova M L 2006 *Appl. Phys. Lett.* **88** 121910
- [12] Hurley D C, Kopycinska-Müller M, Langlois E D, Kos A B and Barbosa N 2006 *Appl. Phys. Lett.* **89** 021911
- [13] Stan G, Ciobanu C V, Parthangal P M and Cook R F 2007 *Nano Lett.* **7** 3691

- [14] Stan G, Ciobanu C V, Thayer T P, Wang G T, Creighton J R, Purushotham K P, Bendersky L A and Cook R F 2009 *Nanotechnology* **20** 035706
- [15] Stan G, King S W and Cook R F 2009 *J. Mater. Sci.* **24** 2960
- [16] Stan G, Krylyuk S, Davydov A V and Cook R F 2010 *Nano Lett.* **10** 2031
- [17] Stan G, Solares S D, Pittenger B, Erina N and Su C 2014 *Nanoscale* **6** 962
- [18] Martin Y, Williams C C and Wickramasinghe H K 1987 *J. Appl. Phys.* **61** 4723
- [19] Zhong Q, Inness D, Kjoller K and Elings V B 1993 *Surf. Sci.* **290** L688
- [20] Magonov S N, Elings V and Whangbo M-H 1997 *Surf. Sci.* **375** L385
- [21] Tamayo J and Garcia R 1997 *Appl. Phys. Lett.* **71** 2394
- [22] Rodriguez T and Garcia R 2004 *Appl. Phys. Lett.* **84** 449
- [23] Proksch R 2006 *Appl. Phys. Lett.* **89** 113121
- [24] Martinez N F, Patil S, Lozano J R and Garcia R 2006 *Appl. Phys. Lett.* **89** 153115
- [25] Solares S D and Chawla G 2010 *J. Appl. Phys.* **108** 054901
- [26] Lozano J R and Garcia R 2008 *Phys. Rev. Lett.* **100** 076102
- [27] Garcia R and Herruzo E T 2012 *Nat. Nanotechnology* **4** 217
- [28] Albrecht T R, Grütter P, Horne D and Rugar D 1991 *J. Appl. Phys.* **69** 668
- [29] Garcia R and Perez R 2002 *Surf. Sci. Rep.* **47** 197
- [30] Albers B J, Schwendemann T C, Baykara M Z, Pilet N, Liebmann M, Altman E I and Schwarz U D 2009 *Nat. Nanotechnol.* **4** 307
- [31] Fukuma T, Ueda Y, Yoshioka S and Asakawa H 2010 *Phys. Rev. Lett.* **104** 016101
- [32] Killgore J P and Hurley D C 2012 *Appl. Phys. Lett.* **100** 053104
- [33] Gates R S and Pratt J R 2012 *Nanotechnology* **23** 375702
- [34] Gates R S, Osborn W A and Pratt J R 2013 *Nanotechnology* **24** 255706
- [35] Warfield R W, Cuevas J E and Barnet F R 1968 *J. Appl. Polym. Sci.* **12** 1147
- [36] Derjaguin B V, Müller V M and Toporov Y P 1975 *J. Colloid Interface Sci.* **53** 314
- [37] Johnson K L, Kendall K and Roberts A D 1971 *Proc. R. Soc. A* **324** 301
- [38] Maugis D 1992 *J. Colloid Interface Sci.* **150** 243
- [39] Carpick R W, Ogletree D F and Salmeron M 1999 *J. Colloid Interface Sci.* **211** 395
- [40] Schwarz U D 2003 *J. Colloid Interface Sci.* **261** 99
- [41] Wahl K J, Asif A S, Greenwood J A and Johnson K L 2006 *J. Colloid Interface Sci.* **296** 178
- [42] Greenwood J A and Johnson K L 2006 *J. Colloid Interface Sci.* **296** 284
- [43] Stafford C M, Harrison C, Beers K L, Karim A, Amis E J, VanLandingham M R, Kim H-C, Volksen W, Miller R D and Simonyi E E 2004 *Nat. Mater.* **3** 545